THE AMERICAN SOCIETY OF MECHANICAL ENGINEERS
345 E. 47th St., New York, N.Y. 10017

95-GT-331

VANE SWIRLER PERFORMANCE

David G. Lilley*
School of Mechanical and Aerospace Engineering
Oklahoma State University
Stillwater, OK 74078

ABSTRACT

Swirler performance characteristics are investigated under low speed, low turbulence intensity conditions so as to aid in computer modeling of flowfields, and in the development and evaluation of turbulence models for swirling confined flow. The swirler studied is annular with a hub-to-swirler diameter ratio of 0.25 and ten adjustable vanes of pitch-to-chord ratio 0.68. Measurements of time-mean axial, radial, and swirl velocities are made at the swirler exit plane using a five-hole pitot probe technique with computer data reduction. A theoretical study is included of idealized exit-plane velocity profiles relating the swirl numbers S and S' to the ratio of maximum swirl and axial velocities for each idealized case. The time-mean velocity components measured at the swirler exit plane show clearly the effects of centrifugal forces, recirculation zones, and blade wakes on the exit-plane velocity profiles. Assumptions of flat axial and swirl profiles are found to be progressively less realistic as the swirl vane angle increases, with axial and swirl velocities peaking strongly at the outer edges of the swirler exit and significant non-zero radial velocities present. Nonaxisymmetry is present in all swirl cases investigated.

NOMENCLATURE

c	blade chord width
d	swirler exit diameter
D	test section diameter
F	velocity ratio w_o/u_o for case I
G	axial flux of momentum; velocity ratio w_{mo}/u_o for case II
H,I,J	w_{mo}/u_o for cases III - V
p	time-mean pressure
s	blade spacing or pitch
S	swirl number = $G_\theta/(G_x\ d/2)$
u,v,w	axial, radial and swirl components of velocity
x,r,θ	axial, radial, azimuthal cylindrical polar coordinate
z	hub-to-swirler diameter ratio d_h/d
θ	azimuth angle
ρ	density
σ	pitch-to-chord ratio = s/c
ϕ	swirl vane angle

SUBSCRIPTS

h	hub
in	inlet conditions, upstream of swirler
m	maximum profile value
o	value at swirler outlet
x	axial direction
θ	tangential direction
∞	reference value at edge of swirler exit

SUPERSCRIPTS

alternate form, neglecting pressure variation; fluctuating quantity time-mean quantity

1. INTRODUCTION

The need for a more complete understanding of the fluid dynamics of the flow in combustion chambers has been recognized by designers in recent years, and research is continuing on several fronts to alleviate the problem. Recent textbooks describe and discuss pertinent issues, see for example: Beer & Chigier (1972), Lefebvre (1983), Gupta et. al (1984), Gupta & Lilley (1985), Chomiak (1990), Chigier (1991), and Keating (1993). The present research project was concerned with experimental and theoretical research in 2-D axisymmetric geometries under low speed, non-reacting, turbulent, swirling flow conditions. The flow enters the test section and proceeds into a larger chamber (the expansion ratio D/d = 2) via a sudden or gradual expansion

---

* Professor, School of Mechanical and Aerospace Engineering

Presented at the International Gas Turbine and Aeroengine Congress and Exposition
Houston, Texas - June 5-8, 1995

(side-wall angle α = 90 and 45 degrees). Inlet swirl vanes are adjustable to a variety of vane angles with ϕ = 0, 38, 45, 60 and 70 degrees being emphasized. The general aim of the entire study was to characterize the time-mean and turbulence flowfield, recommend appropriate turbulence model advances, and implement and exhibit results of flowfield predictions.

Research has progressed in several areas related to the flow facility just described, with flow visualization, pitot probe and hot-wire measurements, and associated computer simulation and turbulence modeling studies. Lilley (1986a) reviews the studies related to axisymmetric flowfields; Lilley (1986b) reviews the studies related to one and two laterally injected jets into the flowfield. Accuracy of predictions from a computer model is strongly dependent on the inlet boundary conditions used, which are primarily determined by the swirler and its performance at different vane angle settings. Measurements taken close to the swirler exit show that the profiles produced are quite nonuniform, with nonzero radial velocity and nonaxisymmetry of axial and swirl velocities. This is in contrast to the "idealized" flat profiles of axial and swirl velocity sometimes used, with zero radial velocity. The present contribution concentrates on the time-mean flow characteristics being generated by the upstream annular swirler, using a five-hole pitot probe technique, under low speed, low turbulence intensity conditions.

2. THEORETICAL ANALYSIS

2.1 Idealized Velocity Profiles

Common assumptions made about swirler performance include flat axial and swirl velocity profiles downstream of the swirler for swirlers with vanes of constant angle and a flat axial profile with a linear swirl profile (solid-body rotation) for swirlers with helicoidal vanes and for tangential-entry swirl generators. These, however, have been found to be quite unrealistic, see for example: Kerr & Fraser (1965), Mather & MacCallum (1967), Chigier & Chervinsky (1967), Beltagui & MacCallum (1976), Sander (1983), and Bulzan (1994). Use of idealized profiles is also unwise when used as inlet conditions to a computer prediction of the combustor flowfield downstream of the inlet swirler, see for example: Rhode et. al (1982), Abujelala & Lilley (1984), and Lilley (1986a). Although the best remedy for numerical simulations is to used experimentally measured swirler exit profiles if they are available, idealized profiles are very useful in theoretical work. If more realistic profile assumptions can be developed which are still mathematically tractable, more useful simulation results may be derived. Better idealized profiles would also be useful as inlet boundary conditions for computer modeling when measured data are not available.

Several combinations of linear and parabolic idealized profiles are shown in Fig. 1, along with the flat, linear and parabolic profile assumptions stated in the form of profile expressions. Parameters associated with these profiles are investigated in Section 2.3.

2.2 Definition of Swirl Parameters

The swirl number is a nondimensional parameter used to characterize the degree of swirl generated by a swirler. It is defined as

$$S = \frac{G_\theta}{G_x(d/2)} \tag{1}$$

where the axial flux of angular momentum G_θ is given by

$$G_\theta = \int_0^{2\pi} d\theta \int_0^{d/2} [\rho uw + \overline{\rho u'w'}]\, r^2\, dr \tag{2}$$

and the axial flux of axial momentum G_x is given by

$$G_x = \int_0^{2\pi} d\theta \int_0^{d/2} [\rho u^2 + \overline{\rho u'^2} + (p - p_\infty)]\, r\, dr \tag{3}$$

and d/2 is the swirler exit radius. These equations are obtained from appropriate manipulation of the axial and azimuthal momentum equations, respectively. In free jet flows these two expressions are invariant with respect to downstream location. In the axial momentum expression, the pressure term $(p - p_\infty)$ is given from radial integration of the radial momentum equation by

$$(p - p_\infty) = \int_{d/2}^{r} \left[\rho w^2 \frac{1}{r}\right] dr - \overline{\rho v'^2} \tag{4}$$

If the pressure term is omitted from the axial momentum, the dynamic axial momentum flux G_x' is obtained:

$$G_x' = \int_0^{2\pi} d\theta \int_0^{d/2} [\rho u^2 + \overline{\rho u'^2}]\, r\, dr \tag{5}$$

and leads to an alternate definition of swirl number:

$$S' = \frac{G_\theta}{G_x'(d/2)} \tag{6}$$

If turbulent stress terms are neglected, it is apparent that a knowledge of the distribution of the time-mean u and w velocity components across the swirler is sufficient to calculate either swirl number. The idealized exit velocity profiles provide just such knowledge, and expressions relating swirl number to the ratio of maximum exit swirl velocity to maximum or constant axial velocity can now be derived for each of the profile types. As the procedure is similar for each of the five cases, a detailed derivation is shown for the first case only, with results merely stated for the other four cases.

2.3 Swirl Numbers for Idealized Profiles

By assuming axisymmetric flow and neglecting turbulent stresses as stated previously, the definitions in Eqs. (2) through (4) reduce to

$$G_\theta = 2\pi \int_0^{d/2} [\rho uw] r^2\, dr \tag{7}$$

$$G_x = 2\pi \int_0^{d/2} [\rho u^2 + (p - p_\infty)] r\, dr \tag{8}$$

$$(p - p_\infty) = \int_{d/2}^{r} \left[\rho w^2 \frac{1}{r}\right] dr \tag{9}$$

When the expressions for axial and swirl velocity for case I (See Fig. 1) are substituted into Eq. (7), one obtains

$$G_\theta = \frac{2}{3}\pi\rho u_o w_o (d/2)^3 \tag{10}$$

Substitution of $w(r) = w_o$ into Eq. (9) and integrating produces

$$(p - p_\infty) = \rho w_o^2 [1n(r) - 1n(d/2)] \tag{11}$$

After substituting Eq. (11) into Eq. (8) and integrating, the expression becomes

$$G_x = \pi\rho u_o^2 (d/2)^2 \left[1 - \frac{1}{2}\left(\frac{w_o}{u_o}\right)^2\right] \tag{12}$$

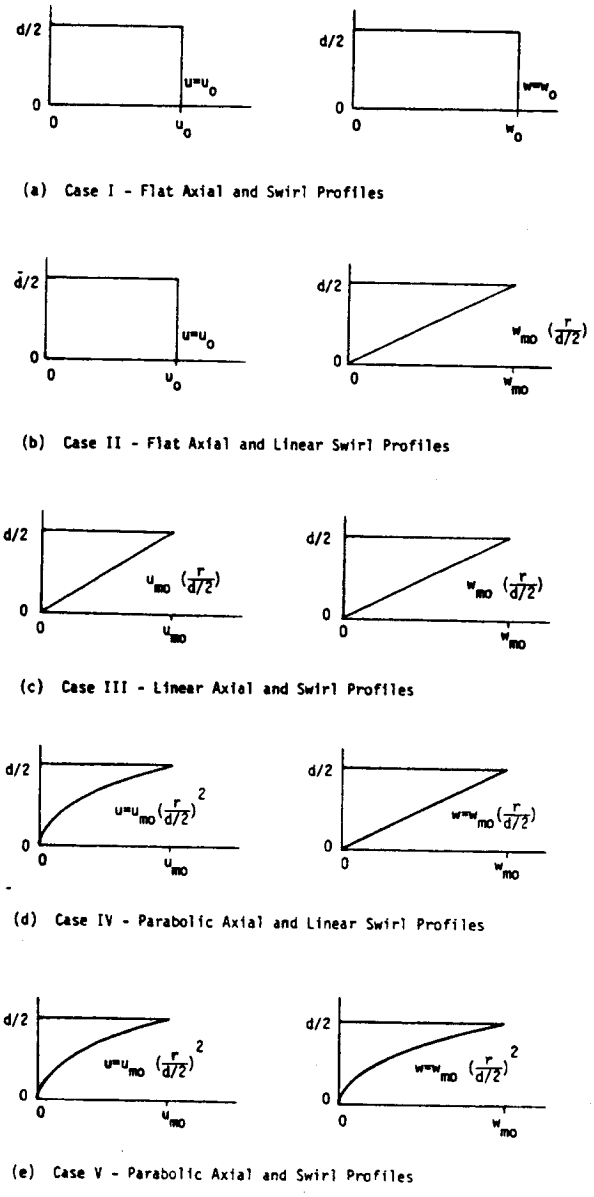

Fig. 1. Idealized axial and swirl velocity profile cases

Finally, putting Eqs. (10) and (12) into Eq. (1) and defining the velocity ratio $F = w_o/u_o$, the swirl number S can be expressed thus:

$$S = \frac{2F/3}{1 - F^2/2} \tag{13}$$

The alternate swirl number S' follows from finding the dynamic axial flux of axial momentum:

$$G_x' = \pi\rho u_o^2 (d/2)^2 \tag{14}$$

Using this in Eq. (6) leads to the simple expression

$$S' = 2F/3 \tag{15}$$

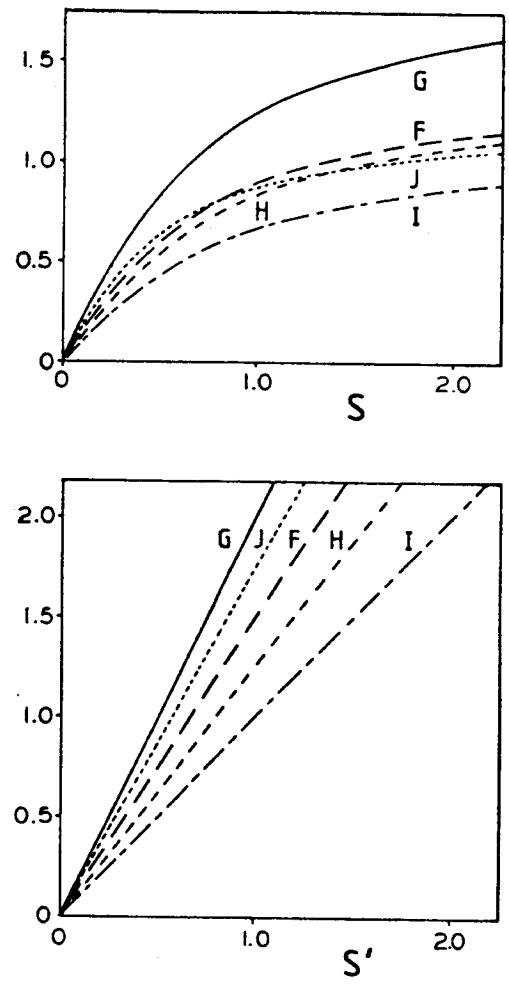

Fig. 2. Variation of velocity ratios F through J [Cases I through V, respectively] with S and S'.

Equations (13) and (15) provide the top row in Table 1, where equations relating S and S' to F, G, H, I, and J [deduced in a similar manner] are given for the five cases of Fig. 1. Note that the profile equations are given in Fig. 1 and other parameters are defined by:

$$\begin{aligned} F &= w_o/u_o \\ G &= w_{mo}/u_o \\ H &= w_{mo}/u_{mo} \\ I &= w_{mo}/u_{mo} \\ J &= w_{mo}/u_{mo} \end{aligned} \qquad (16)$$

It is interesting to see how these parameters vary with S and S', and Fig. 2 portrays the relationships of the equations in Table 1 visually, for a range of commonly encountered swirl numbers.

Table 1. Idealized Swirler Exit Velocity Profiles

Case	S	S'
I	$S = \frac{2F/3}{1 - F^2/2}$	$S' = 2F/3$
II	$S = \frac{G/2}{1 - G^2/4}$	$S' = G/2$
III	$S = \frac{4H/5}{1 - H^2/2}$	$S = 4H/5$
IV	$S = \frac{I}{1 - 3I^2/4}$	$S' = I$
V	$S = \frac{4J/7}{1 - 2J^2/3}$	$S' = 4J/7$

3. EXPERIMENTAL EQUIPMENT AND PROCEDURE

3.1 The Facility

The installation on which all tests were performed is a low-speed wind tunnel designed and built at Oklahoma State University. It produces uniform low speed flow of relatively low turbulence intensity, with continuously adjustable flow rate. The facility consists of a filtered intake, an axial blower, a stilling chamber, a turbulence management section, and a contoured outlet nozzle. It is described at length in Lilley (1986a). The contoured nozzle is made of molded fiberglass with a steel flange at the outlet for the attachment of the swirler and/or expansion block en route to the test section in associated studies. A 1 cm diameter hole a short distance upstream of the outlet allows for insertion of a standard pitot-static probe to measure the dynamic pressure upstream of the swirler. This measurement, with a small correction for difference in flow area, is used to calculate the swirler inlet reference velocity, u_{in}.

3.2 The Swirler

The swirler used in this study is annular with hub and housing diameters of 3.75 and 15.0 cm, respectively, giving a hub-to-swirler diameter ratio z of 0.25. The hub has a streamlined parabolic nose facing upstream and a blunt base (corner radius approximately 2 mm) facing downstream. It is supported by four thin rectangular-sectioned struts or spider arms from the housing wall. The base of the hub protrudes approximately 3 mm downstream of the swirler exit plane. A schematic of the swirler is shown in Fig. 3.

The ten vanes or blades are attached to shafts which pass through the housing wall and allow individual adjustment of each blade's angle. The standard vanes are wedge-shaped to give a constant pitch-to-chord ratio σ of 0.68, which according to two-dimensional cascade data, should give reasonably good flow-turning effectiveness. Sets of vane planforms are shown in Fig. 4.

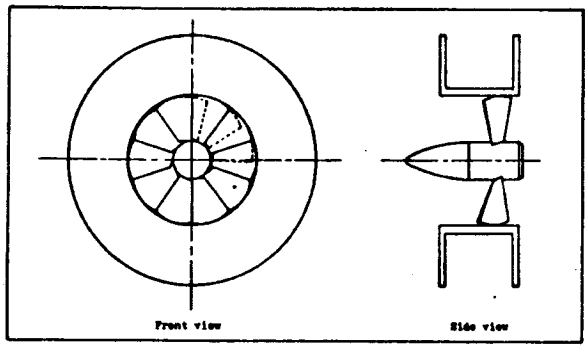

Fig. 3. Diagram of swirler - section and downstream view.

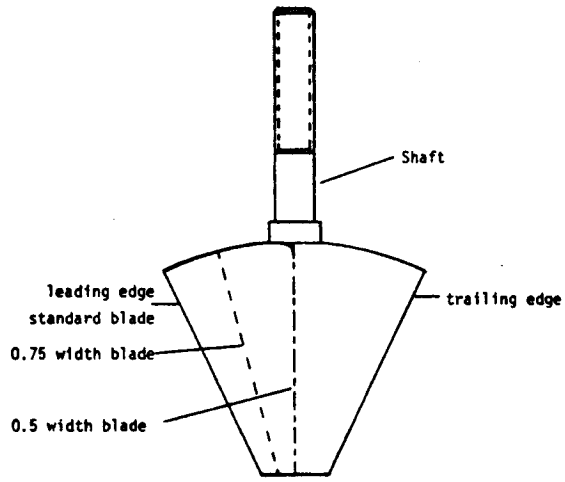

Fig. 4. Swirl vanes.

3.3 Measurement Procedure

The time-mean velocity components are measured with a five-hole pitot probe which allows determination of the magnitude and direction of the mean velocity vector simultaneously. The probe is mounted in a traversing mechanism which allows it to be translated vertically (on a radial line outward from the test section axis) and rotated about the probe's yaw axis. In addition to the motion permitted by the traverse mechanism, the test section tube on which the traverse mechanism is mounted may be rotated

about its axis with respect to the swirler, thereby allowing azimuthal traverses to be performed. Tubing from the probe's five pressure taps is routed through selector valves to a differential pressure transducer, and the resulting pressure difference values are read directly from an integrating digital voltmeter. The pressure data are reduced by a computer program to yield nondimensionalized u, v, and w velocity components, which are then plotted in the form of profiles.

4. EXPERIMENTAL RESULTS

Velocity profiles from both radial and azimuthal traverses for each of the flowfields investigated are now presented and discussed. The radial traverses consist of ten points from the centerline to the swirler exit radius, spaced 7.6 mm apart. Of these ten, only seven stations were actually measured since the hub blocked the inner three positions. A diagram showing the traverse patterns on the face of the swirler is given in Fig. 5. All traverses were taken immediately after the swirler exit downstream face with no expansion blocks present.

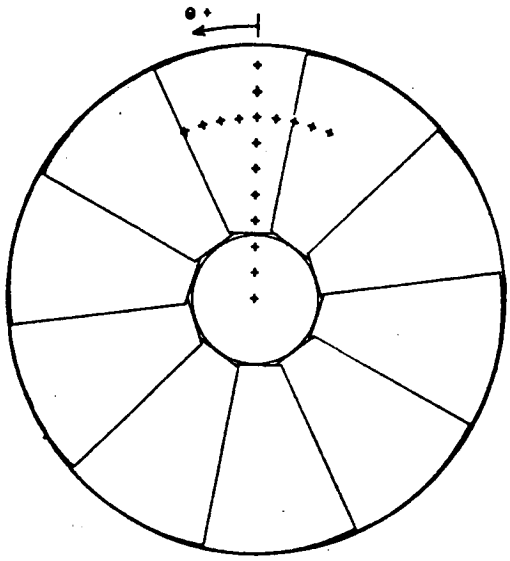

Fig. 5. Measurement locations - radial and azimuthal traverses.

Radial traverses of axial, radial and swirl velocity component data are presented for five values of swirl blade angle: zero (no swirler), zero (with swirler), 38, 45, 60, and 70 degree, in Figs. 6 through 11, respectively, with the profiles extending from the centerline to twice the exit radius (r/D = 0.5 where D is the test section diameter used in associated studies). All velocities shown are normalized with respect to the swirler inlet uniform axial velocity u_{in}, deduced independently from the pitot-static measurement upstream of the swirler. The outer ten data points are zero in each profile because the presence of the solid boundary of the swirler flange precluded measurements at these locations.

The nonswirling case shown in Fig. 6 has a nearly-flat axial velocity profile, as expected for the plain nozzle opening without the swirler installed. There is no measurable swirl velocity, and the radial velocity is zero except for points very near the edge of the exit, where the flow begins to anticipate the abrupt expansion to twice the exit diameter. The second nonswirling case, see Fig. 7, has the swirler installed with the blades set to $\phi = 0$ degree. The traverse was made midway between two blades and away from any of the hub supporting struts. Here again the axial profile is quite flat, with just a slight increase toward the hub. However, the velocity has increased by nearly 25 percent, because of the decrease in flow area with swirler hub and vanes in place. In addition, the hub induces a negative radial velocity across the entire annulus, overriding the tendency to anticipate the expansion corner. The swirl velocity is, as expected, negligible.

The 38-degree blade-angle case in Fig. 8 shows remnants of the flat inlet profile over a small portion of the radius near the outside edge in both the axial and swirl profiles. The presence of the hub now constrains the three innermost points to zero, and the region between the hub and the flat portion in the axial and swirl profiles is approximately linear. The maximum axial velocity is 1.5 times the inlet axial velocity because the flow area is decreased by the hub and also because centrifugal effects have shifted the profile outward. The radial velocity has an irregular profile with a maximum value of one-half the inlet axial velocity.

In the $\phi = 45$ degree case of Fig. 9, the flat segments are no longer present and both axial and swirl profiles vary from zero at the hub to a maximum at or near the rim of the swirler in an almost linear fashion. The similar shape and magnitude of the profiles indicates that the turning angle is fairly uniform and only slightly less than 45 degrees. The radial velocity is again irregular, but shows a step at r/D = 0.1 similar to that in the axial and swirl profiles; this is probably due to the central recirculation zone downstream beginning to slow down the flow upstream of it.

Profiles ensuing from the case of $\phi = 60$ degree, see Fig. 10, all have a sharply peaked shape, with most of the flow leaving near the outer boundary. The radial component is considerably stronger, with a peak value nearly twice that of the reference velocity upstream of the swirler. The step seen previously in the 45 degree axial profile, has now developed into reverse flow, indicating that the central recirculation zone now extends upstream past the exit plane. The reverse flow is accompanied by reduced swirl velocity and very low values of radial velocity. The positive axial velocity adjacent to the hub may be the result of a slight clearance between the blades and the hub, allowing air with greater axial momentum to pass through.

Exit velocity profiles obtained for the strongest swirl case considered ($\phi = 70$ degree) are shown in Fig. 11. Almost all of the flow leaves the swirler at the outside edge. The maximum axial and swirl velocities are approximately 3 and 2.5 times the upstream reference values, respectively, and the velocity gradients across the profiles are quite large. The reverse flow in the center of the axial profile is stronger than in the 60-degree case and is now accompanied by negative or inward radial velocity. This suggests the possibility of a vortex ring structure occurring at the exit of the swirler under high-swirl conditions. The swirl velocity profile remains

positive but shows a step corresponding to the outer boundary of the recirculation zone.

An indication of the azimuthal or θ-variation of axial, radial, and swirl velocities is available for the same vane angle settings used in the radial traverses. The data are available in Sander (1983) and Lilley (1986a). The profiles all show significant variation with azimuthal position, except for those in or near recirculation zones where the w-velocity component is dominant. These variations can be attributed to several causes, among them being blade stall from using flat blades at high angles of attack and wakes from blunt trailing edges.

Swirl numbers S and S' were calculated from Eqs. (1) and (6), with the turbulent stress terms omitted. Measured velocities and pressure (with reference pressure p_∞ being at the outer edge of the swirler at r/D = 0.25) from the radial traverses of Section 4.1 were used with appropriate numerical integration. Results are shown in Table 2 where the flat blade swirler exhibits asymptotic behavior in its ability to produce strong swirl. Also shown is the measured ratio w_{mo}/u_{mo} for each swirl vane angle.

Someone unaware of the actual swirler exit velocity and pressure distributions might proceed in the following way. An 'ideal' flat blade swirler operating on a plug flow would produce exit profiles like Case I of Fig. 1 with $F = w_o/u_o = \tan \phi$ where ϕ is the swirl vane angle. Corresponding S and S' values are then found from the equations of Table 1 which are plotted in Fig. 2. These 'idealized theoretical' values are given in Table 3, where negative values occur when the theoretical pressure contribution dominates in the denominator with negative consequences. It may be noticed immediately that the actual swirler performance is considerably inferior to the idealization, and thus observant theorists must continue to use actual test section inlet data in preference to the most simple idealization of Case I.

Table 2. Measured Swirl Numbers

ϕ	S	S'	w_{mo}/u_{mo}
38	0.567	0.559	0.801
45	0.765	0.718	0.876
60	0.850	0.759	0.937
70	0.883	0.750	0.887

Table 3. Theoretical Swirl Numbers

ϕ	Ideal Case I		Most Appropriate Case		
	S	S'	Case	S	S'
38	0.750	0.521	I	0.786	0.534
45	1.333	0.667	III	1.137	0.584
60	-2.309	1.155	V	1.291	0.625
70	-0.660	1.832	V	1.066	0.591

Even the other less idealized 'theoretical' cases are also inappropriate. The latter part of Table 3 gives the calculated swirl strengths on the basis of the most appropriate profiles (Cases I through V of Section 2.3) with associated F through J values taken from the measurements (values are given in Table 3). These disparities are attributed to the presence of the central hub, the upstream extent of the central recirculation zone, and flat swirl-vane ineffectiveness at high angles of attack, with associated wakes and nonaxisymmetries.

5. CONCLUSIONS

A theoretical analysis of swirl number associated with several idealized exit velocity profiles was included, and values of the ratio of maximum swirl velocity to maximum axial velocity at different swirl strengths are given for each case. Measurements of actual swirler exit velocity profiles were made for swirl vane angles ϕ = 0, 38, 45, 60, and 70 degrees using a five-hole pitot probe technique. Assumptions of flat axial and swirl profiles with radial velocity equal to zero were found to be progressively less realistic as the swirler blade angle increases. These data form a useful part of a data base for the evaluation of flowfield prediction codes and turbulence models.

REFERENCES

Abujelala, M.T., and Lilley, D.G. (1984), "Swirler Performance and Confined Swirling Flow Predictions", Proc. ASME Computers in Engng. Conf., Las Vegas, NV, Aug. 12-15, 1984, pp. 233-241.

Beer, J.M., and Chigier, N.A. (1972), "Combustion Aerodynamics", Applied Science Publishers, London.

Beltagui, S.A., and MacCallum, N.R.L. (1976), "Aerodynamics of Vane-Swirled Flames in Furnaces", Journal of the Inst. of Fuel, Vol. 49, Dec., pp. 183-193.

Bulzan, D. L. (1994), "Structure of a Swirl-Stablized Combusting Spray", NASA TM 106724, August, 1994.

Chigier, J. (1991), "Combustion Measurements", Hemisphere Publishing Corp., New York.

Chigier, N.A., and Chervinsky, A. (1967), "Experimental Investigation of Swirling Vortex Motion in Jets", Journal of Applied Mechanics, Vol. 34, June 1967, pp. 443-451.

Chomiak, J. (1990), "Combustion: A Study in Theory, Fact and Application", Abacus Press/Gordon & Breach, New York.

Gupta, A.K., and Lilley, D.G. (1985), "Flowfield Modeling and Diagnostics", Abacus Press, Tunbridge Wells, England.

Gupta, A.K., Lilley, D.G., and Syred, N. (1984), "Swirl Flows", Abacus Press, Tunbridge Wells, England.

Keating, E.L. (1993), "Applied Combustion", Marcel Dekker, New York.

Kerr, N.M., and Fraser, D. (1965), "Swirl. Part I: Effect on Axisymmetrical Turbulent Jets", Journal of the Inst. of Fuel, Vol. 38, Dec., pp. 519-526.

Lefebvre, A.H. (1983), "Gas Turbine Combustion", McGraw Hill, New York.

Lilley, D.G. (1986a), "Swirling Flows in Typical Combustor Geometries", Journal of Propulsion and Power, Vol. 2, No. 1, Jan.-Feb., pp. 64-72.

Lilley, D.G. (1986b), "Lateral Jet Injection into Typical Combustor Flowfields", NASA CR-3997, July.

Mathur, M.L., and MacCallum, N.R.L. (1967), "Swirling Air Jets Issuing from Vane Swirlers. Part I: Free Jets; Part II: Enclosed Jets", Journal of the Inst. of Fuel, Vol. 40, May, pp. 214-245.

Rhode, D.L., Lilley, D.G., and McLaughlin, D.K. (1982), "On the Prediction of Swirling Flowfields Found in Axisymmetric Combustor Geometries", ASME Journal of Fluids Engng., Vol. 104, pp. 378-384.

Sander, G.F. (1983), "Axial Vane-Type Swirler Performance Characteristics", M.S. Thesis, School of Mechanical and Aerospace Engineering, Oklahoma State University, Stillwater, Okla., May.

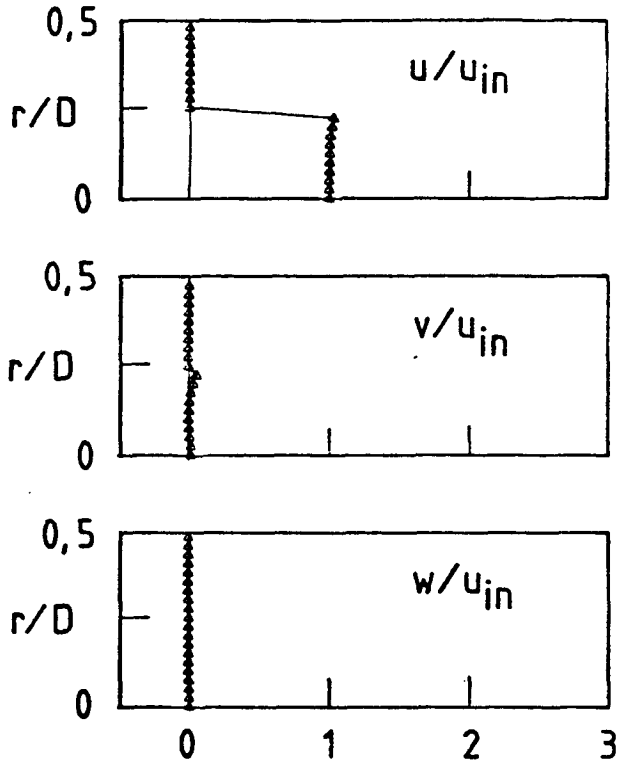

Fig. 6. Normalized velocity profiles from radial traverse, ϕ = 0 degree. (No swirler)

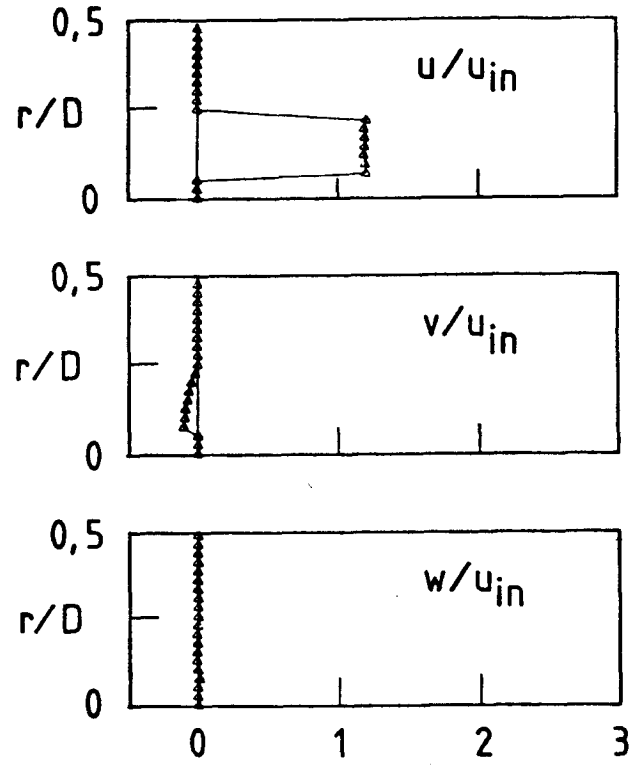

Fig. 7. Normalized velocity profiles from radial traverse, ϕ = 0 degree. (Swirler installed)

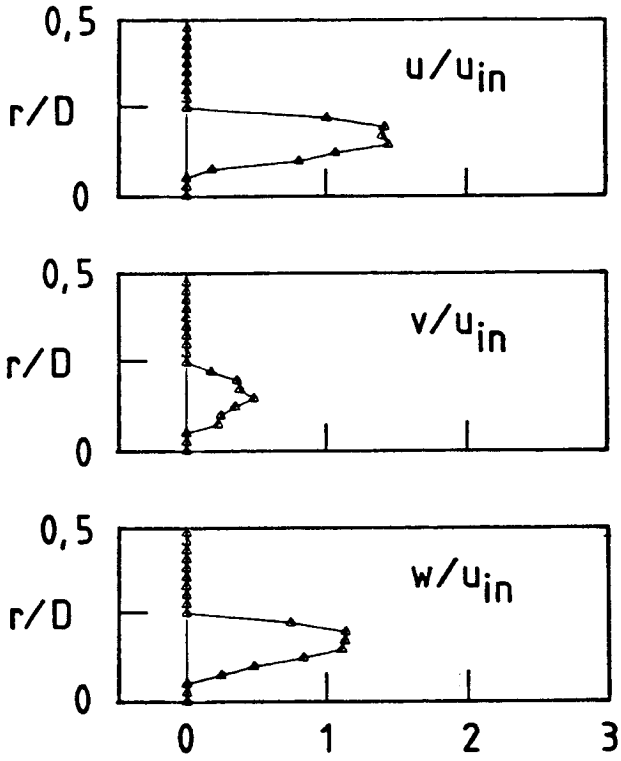

Fig. 8. Normalized velocity profiles from radial traverse, ϕ = 38 degree.

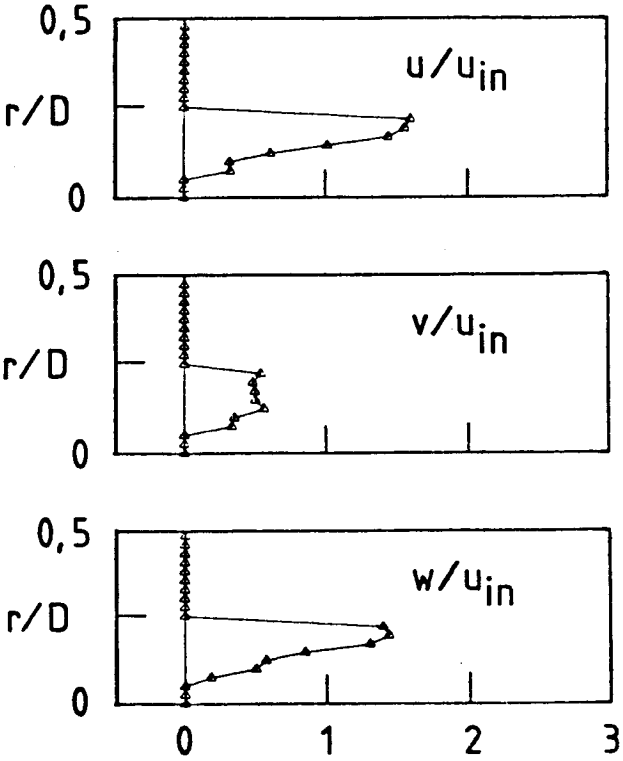

Fig. 9. Normalized velocity profiles from radial traverse, ϕ = 45 degree.

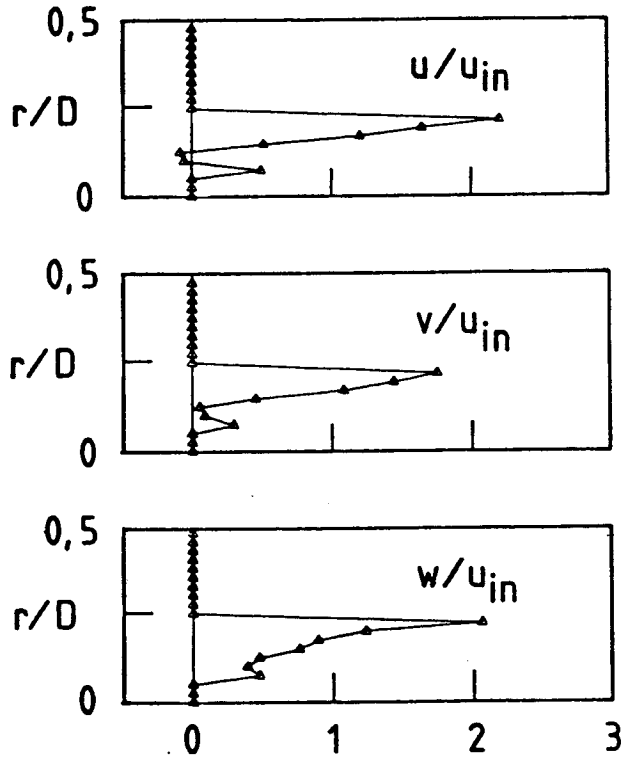

Fig. 10. Normalized velocity profiles from radial traverse, ϕ = 60 degree.

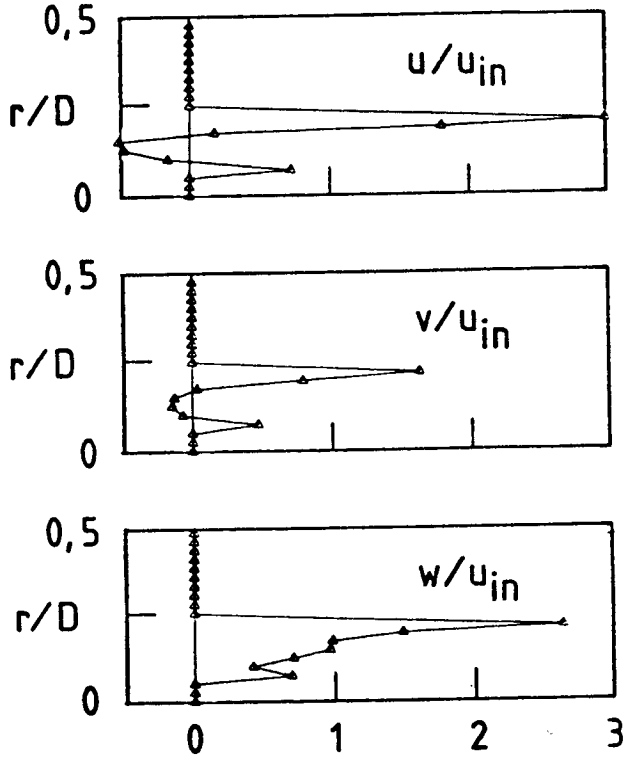

Fig. 11. Normalized velocity profiles from radial traverse, ϕ = 70 degree.